Electronic supplementary information

Nitrogen-doped WSe_2 few-layer nanotubes for electrocatalytic nitrate reduction via Se vacancies

Mingming Tu, Danpeng Lyu, Yifei Li, and Yiwei Tan*

State Key Laboratory of Materials-Oriented Chemical Engineering, School of Chemistry and Chemical Engineering, Nanjing Tech University, Nanjing 211816, China, Email: ytan@njtech.edu.cn

Materials

Sodium tungstate dihydrate ($Na_2WO_4 \cdot 2H_2O$, ≥ 99.0%), selenium powder (100 mesh, ≥99.5%), oleylamine (70%), acetonitrile (≥99.5%), oleic acid (90%), and glacial acetic acid (CH_3COOH, 99.0%) were purchased from Merck. Hydrazine hydrate (85 wt%), anhydrous ethanol (99.5%), sodium nitrate ($NaNO_3$, 99+%), sodium nitrite ($NaNO_2$, 99.99%), nitric acid (68–70%), ammonium chloride (99+%), and isopropanol (99.5%) were commercially available from Thermo Fisher Scientific. Ultrapure water (18.2 MΩ) produced with a Milli-Q purification system was used in the synthesis and physical measurements. Carbon fiber paper (CFP, ~180 μm in thickness) was purchased from Wuhan Cetech Co., Ltd.. A massive piece of CFP was cut into equal parts (1 cm × 3 cm), subsequently rinsed with isopropanol and water in turn three times by sonication, and then pretreated with concentrated nitric acid (68–70%) at the 75 °C for 90 min to achieve the surface hydroxylation of CFP. After being washed with water, the pretreated CFP was used as the support for epitaxially growing hexagonally structured WO_3, WSe_2, and N-WSe_2 nanomaterials.

Characterization

The XRD patterns were acquired at a step length of 0.02° using a Rigaku Smartlab diffractometer with Cu K_α radiation (λ = 1.5406 Å) operating at 40 kV and 100 mA at a scanning rate of 0.06° sec^{-1}. Scanning electron microscopy (SEM) images were obtained using a Hitachi S-4800 field-emission scanning electron microscope operating at 5 kV. Transmission electron microscopy (TEM) micrographs were obtained using a FEI Tecnai G2 Spirit Bio TWIN transmission electron microscope operating at an accelerating voltage of 120 kV. High resolution TEM (HRTEM) and scanning TEM (STEM) micrographs, high-angle annular dark field (HAADF)-STEM-energy-dispersive X-ray spectroscopy (EDX) elemental maps, and EDX spectra were acquired using a FEI ETEM Titan G2 60-300 Cs-corrected scanning transmission electron microscope equipped with a spherical aberration corrector for the electron beam and an energy-dispersive spectrometer (APOLLO XLT SDD system from EDAX) for chemical composition analysis operating at an accelerating voltage of 300 kV. STEM micrographs and EDX elemental maps were obtained in HAADF mode. The specimens for TEM and HRTEM observations were carefully scratched from the CFP substrate and gently sonicated before dropping them onto 300 mesh carbon-coated copper grids. UV–vis–NIR extinction spectroscopy was recorded using a Shimadzu UV-3600 UV–vis–NIR spectrophotometer. The colloidal samples were prepared by dispersing 9 mg of N-SeW_2 or WSe_2 nanotubes into a mixed solvent consisting of n-hexane (3 mL), oleylamine (0.3 mL), and oleic acid (0.3 mL) by vigorously sonicating the dispersion for ca. 50 min using a 120 Hz/100 W sonicator. Electron spin resonance (ESR) signal was obtained using a Bruker A200-6/1 EPR spectrometer at 300 K. The g value was calculated according to the equation $g = h\nu/\beta B$, where h is the Planck constant, ν is the microwave frequency and is 9874.8 MHz, β is the Bohr magneton (9.2740×10^{-24} J T^{-1}), and B is the corresponding magnetic field intensity in a unit of Gauss (1 Gauss = 0.1 mT). Raman spectra were recorded by using the HORIBA-Jobin-Yvon LabRAM HR Evolution Raman spectrometer with an excitation power of 2 mW and integration time of 0.05 s (excitation wavelength: 514 nm). The laser was focused on the samples with a confocal microscope equipped with a 50X long working distance objective (Olympus BX-30-LWD) for the visible lasers. The samples (*ca*. 10 mg of loose powder) were placed on a glass slide underneath the objective. For the acquisition of Raman spectra, the accumulation was collected over a period of 10 s per scan for 5 scans with a 500 μm opening for the laser light. X-ray photoelectron spectroscopy (XPS) measurements were

performed on a Kratos Axis Supra (Kratos Analytical, Shimadzu Group Company) spectrometer at 15 kV and 10 mA with a 180° double focusing hemispherical energy analyzer providing energy resolution of 0.1 eV, employing a monochromatized microfocused Al-K_α ($h\nu$ = 1486.58 eV) X-ray source with 600 W X-ray power. The binding energy (BE) for the samples was calibrated by setting the measured BE of C 1s to 284.8 eV. Specimens for XPS measurements were pretreated by repeated cycles of Ar^+ ion sputtering to obtain clean surfaces of the specimens. Survey spectra of the samples in the BE range of 0–1000 eV and the core level spectra of the elemental signals were recorded at resolutions of 1 and 0.1 eV, respectively. The surface chemical compositions were estimated based on the integration of peak areas through deconvolution and fitting the raw data after a Shirley background subtraction.

In situ Raman spectroscopy

In situ Raman spectroscopy measurements were carried out using an alpha300R spectrometer (WITec GmbH) integrated with a confocal Raman microscope. The spectra were recorded by excitation with an Ar^+ ion laser with a wavelength of 532 nm and an output power set as 40 mW. The laser light was focused onto the sample through a 100× oil immersion objective whose numerical aperture is 0.9 (Carl Zeiss). The 180° backscattered Raman signal was transmitted to a spectrometer equipped with a 3000 g mm^{-1} grating (UHTS 300 WITec) through an optic multifibre with a diameter of 50 μm and then detected by a CCD camera (Andor DU401 BV). On the selected areas (30 μm × 20 μm) at the interface of sample and electrolyte, Raman spectrum was acquired every 0.5 μm with an integration time of 1 s in a wavenumber range of 100−1500 cm^{-1}. A Control Five acquisition software (WITec GmbH) was used for the Raman measurements set up and a Project Five (WITec GmbH) to reconstruct Raman images based on the integral bands of the ester group at 1734 cm^{-1} and hydroxyl group at 3400 cm^{-1}.

Quantification of NH_4^+

The concentration of the NH_4^+ produced in the electrolyte was evaluated by a modified indophenol blue method.[1] The reacted electrolyte was diluted 100 times prior to chromogenic reaction. Afterwards, 25 mL of diluted cathodic electrolyte obtained after electrolysis, 1 mL of liquified phenol solution in ethanol (11.1%, v/v), 1 mL of sodium nitroprusside solution (0.5%, w/v), and 2.5 mL of oxidizing solution containing trisodium citrate dihydrate (0.544 M), sodium hydroxide (0.200 M), and sodium hypochlorite (0.134 M), were thoroughly mixed in a 50-mL Ehrlenmeyer flask. After standing in the dark for 1 h at room temperature, the UV-vis spectrum of the sample solution was recorded in the wavelength range of 550 to 750 nm. Five standard $(NH_4)_2SO_4$ solutions (1.0, 2.0, 3.0, 4.0, and 5.0 μg mL^{-1}) were prepared to plot the calibration graph (*i.e.*, extinction versus concentration of NH_4^+). The blank was also treated as one of the standards. The extinction measured at 640 nm by UV-vis spectroscopy in the same wavelength range (550 to 750 nm) was used to determine the concentration of NH_4^+.

Quantification of NO_2^-

The concentration of NO_2^- was quantitatively analyzed using the N-(1-naphthyl)-ethylenediamine dihydrochloride ($C_{12}H_{14}N_2{\cdot}2HCl$) colorimetric method. First, 1 mL of sulfanilamide ($H_2NC_6H_4SO_2NH_2$, 0.5 wt%)-hydrochloric acid (1 M) solution was mixed with 4 mL of the diluted electrolyte obtained after electrolysis (diluted 50 times). After being left for 10 min, 1 mL of $C_{12}H_{14}N_2{\cdot}2HCl$ solution (0.1 wt%) was added to the preceding solution. After mixing for 30 min, the UV-Vis extinction spectrum of the sample was measured in the wavelength range of 450 to 650 nm to derive the NO_2^- concentration. The calibration curve was obtained using the standard $NaNO_2$ solutions (0.1, 0.2, 0.3, 0.4, 0.5, and 0.6 μg mL^{-1}) and the blank (0 μg mL^{-1}). The maximum absorbance occurs at 540 nm.

Quantification of NO_3^-

To eliminate the interference of nitrite, 1 mL of a hydrochloric acid solution (2.0 M) and 1 mL of an amidosulfonic acid solution (1%, w/v) were mixed with 2 mL of the diluted electrolyte solution obtained after electrolysis (diluted 100 times) under stirring for 20 minutes. Five standard $NaNO_3$ solutions (2.0, 4.0, 6.0, 8.0, and 10.0 μg mL^{-1}) were prepared to plot the calibration curve, which was obtained by measuring the extinction at 220 nm versus the NO_3^- concentration of each standard solution. The blank was also treated as one of the standards. The UV-Vis extinction spectra were recorded in the wavelength range of 200 to 300 nm.

Determination of NH_4^+ yield rate and FE

The average NH_4^+ yield rate ($Y_{NH_4^+}$) was calculated according to the equation in the following:

$$Y_{NH_4^+} = \left(c_{NH_4^+} \times V\right) \times 18 / (t \times A) \quad \text{(S1)}$$

where $c_{NH_4^+}$ is the concentration of measured NH_4^+-N (μg/mL), t is the electrolysis time (h), V is the volume of the electrolyte in the cathode chamber (mL), and A is the working electrode area (cm^2).

FE of NH_4^+ production was calculated by the ratio of electrons used for generating NH_4^+ during the whole electrolysis in terms of the equation in the following:

$$\text{FE} = \left[\left(8 \times F \times c_{NH_4^+} \times V\right) / (18 \times Q)\right] \times 100\% \quad \text{(S2)}$$

where F is the Faradic constant (96485 C mol^{-1}), and Q is the total charge transfer during electrolysis (C).

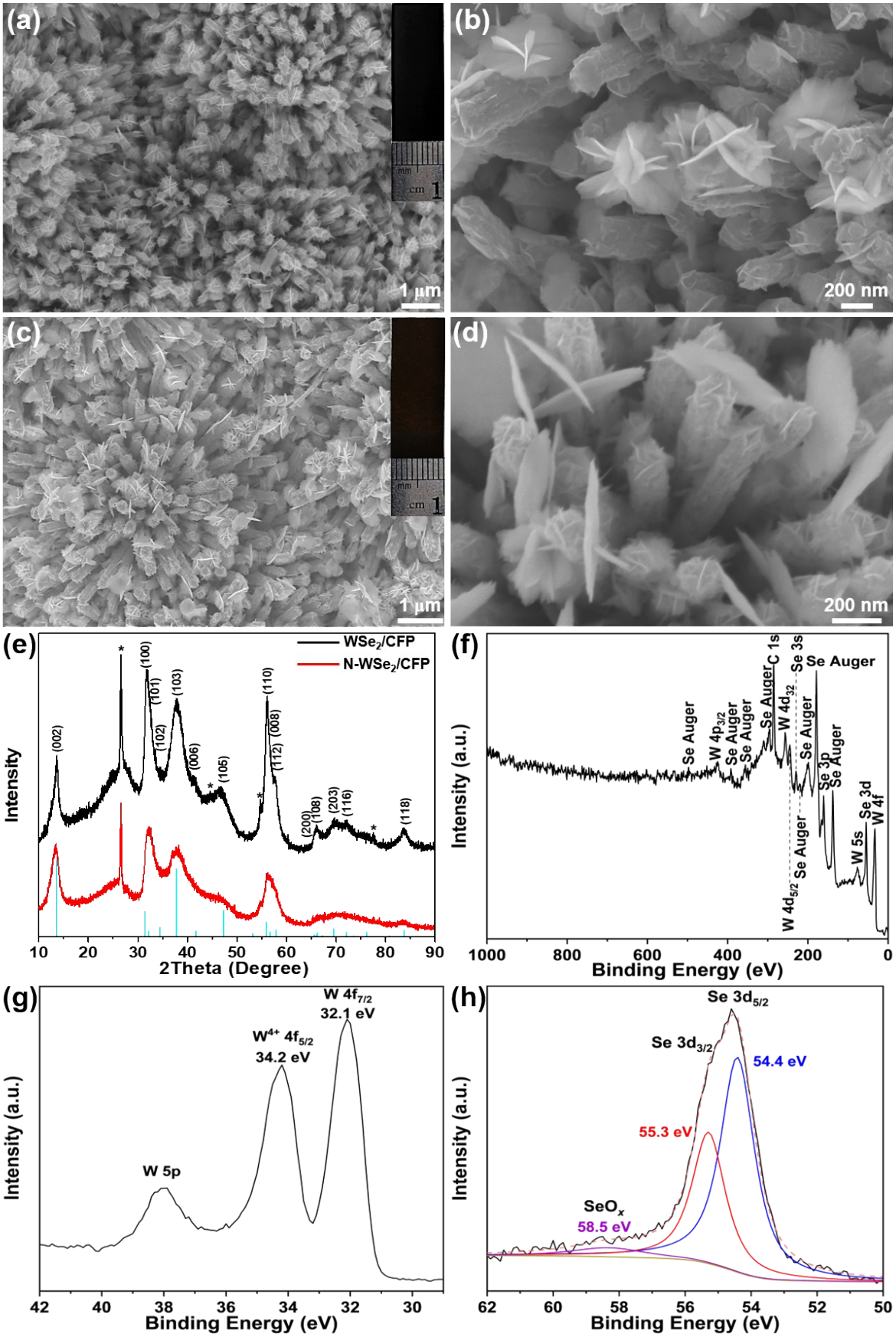

Figure S1. (a and c) Low- and (b and d) high-magnification SEM images, (e) XRD patterns, and (f) XPS survey, (g) W 4f, and (h) Se 3d core-level spectra of (a, b, and f–h) WSe_2/CFP and (c and d) N-WSe_2/CFP (5.1 at.% N). The peaks marked by an asterisk in panel (e) originate from CFP. For comparison, the intensity and position for the

pure WSe_2 reference indicated by the cyan bars are given at the bottom of panel (e) based on the JCPDS database (JCPDF no. 87–2418). Insets: a digital photograph of a piece of (a) the WSe_2/CFP and (c) N-WSe_2/CFP electrode.

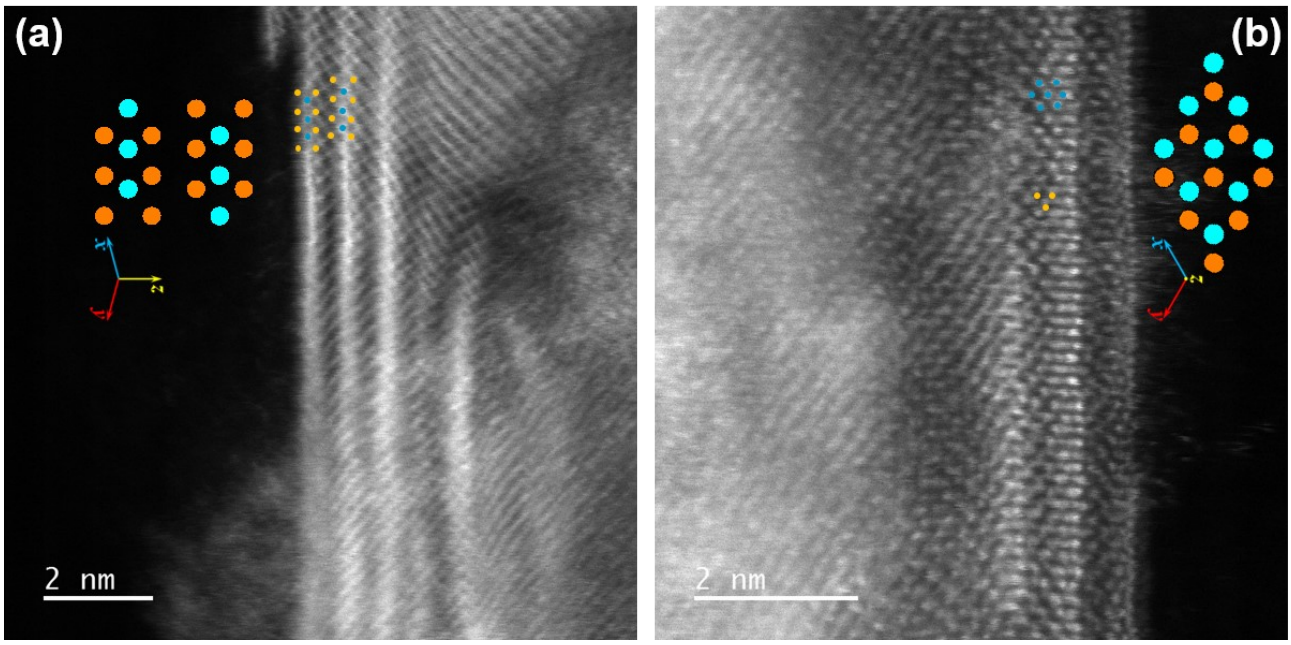

Figure S2. HRTEM images of (a) the stacking of layers and (b) nanotubular walls of the N-WSe_2 NTs. The insets show the atomic arrays of WSe_2 viewed from (a) [110] and (b) [001] directions. The cyan and orange atoms are assigned to W and Se atoms, respectively.

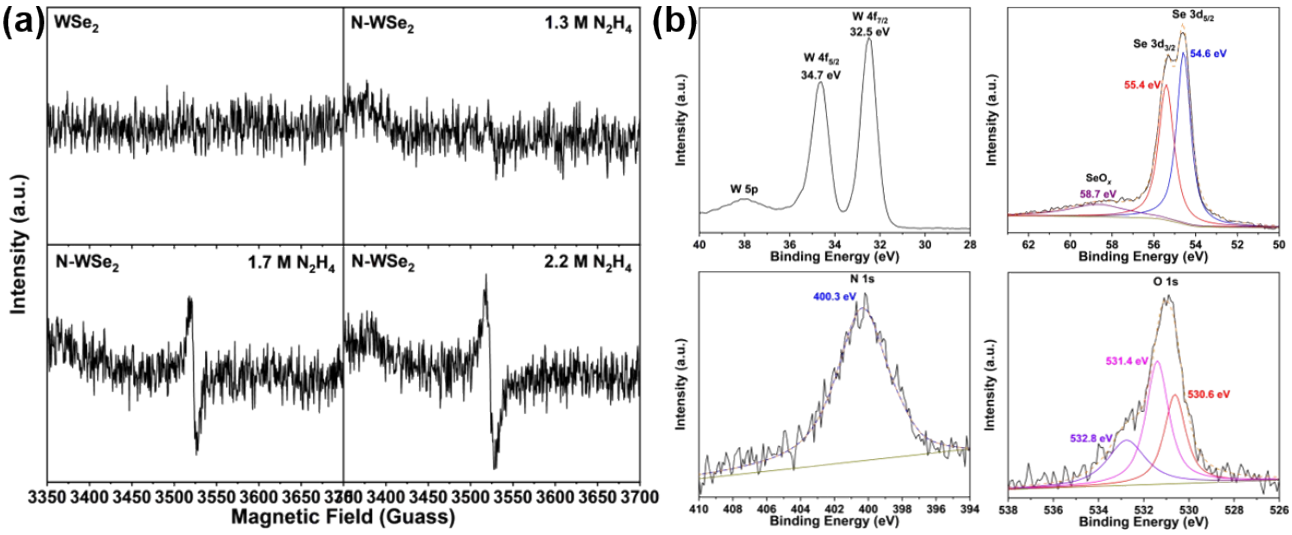

Figure S3. (a) Room-temperature ESR spectra of the various pristine N-WSe_2 NTs and (b) XPS spectra of the N-

WSe_2 NTs (5.1 at.% N) prior to the annealing treatment in a H_2/Ar (5%, v/v) stream.

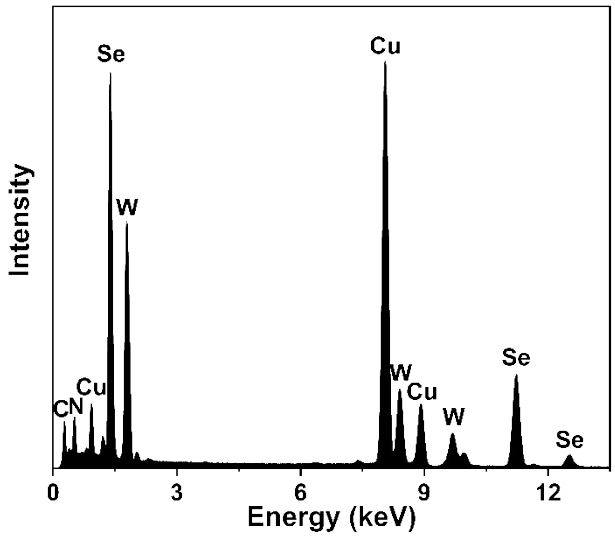

Figure S4. EDX spectrum of the few-layer N-WSe_2 NTs (5.1 at.% N).

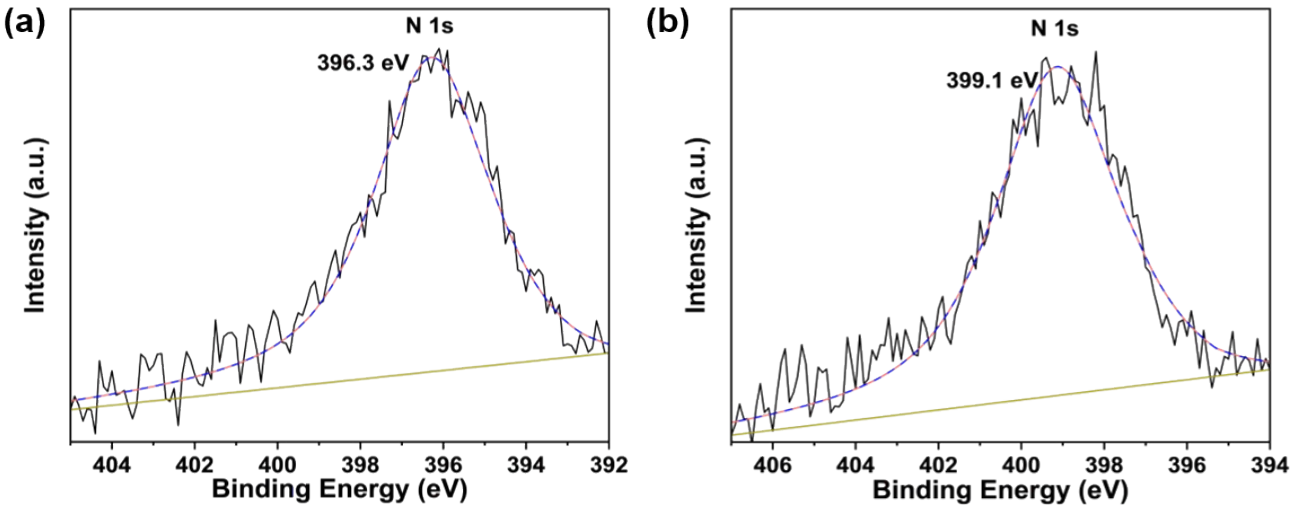

Figure S5. The high-resolution N 1s XPS core-level spectra of (a) the N-WSe_2 (2.7 at.% N) and (b) N-WSe_2 (3.5 at.% N) NTs.

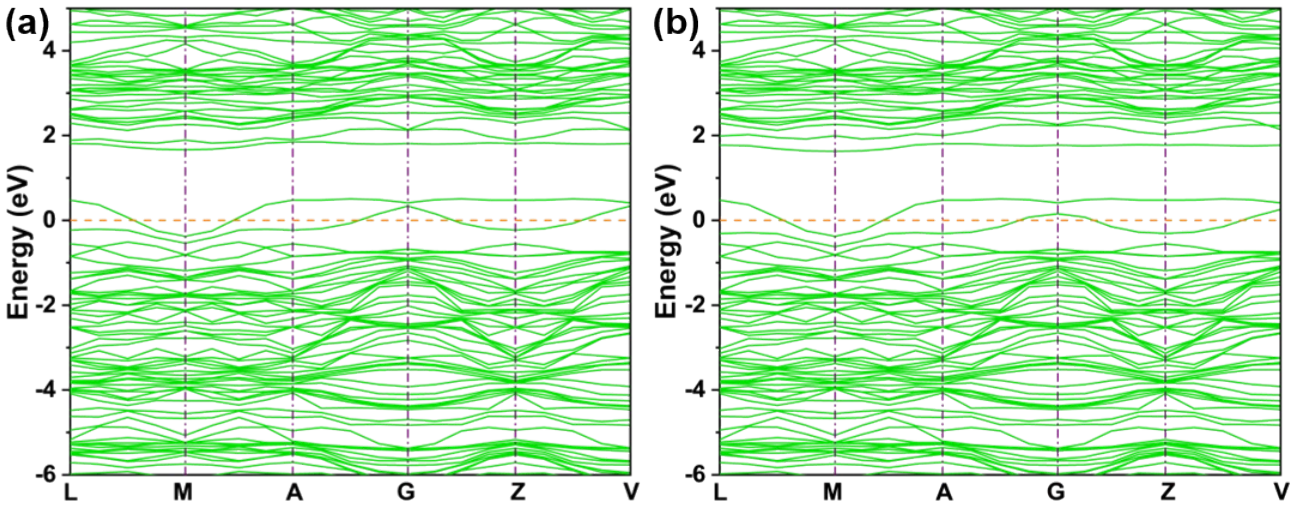

Figure S6. Computed band structures of the N-WSe_2 with (a) 3.5 at.% N and (b) 5.1 at.% N. The Fermi level is set as zero.

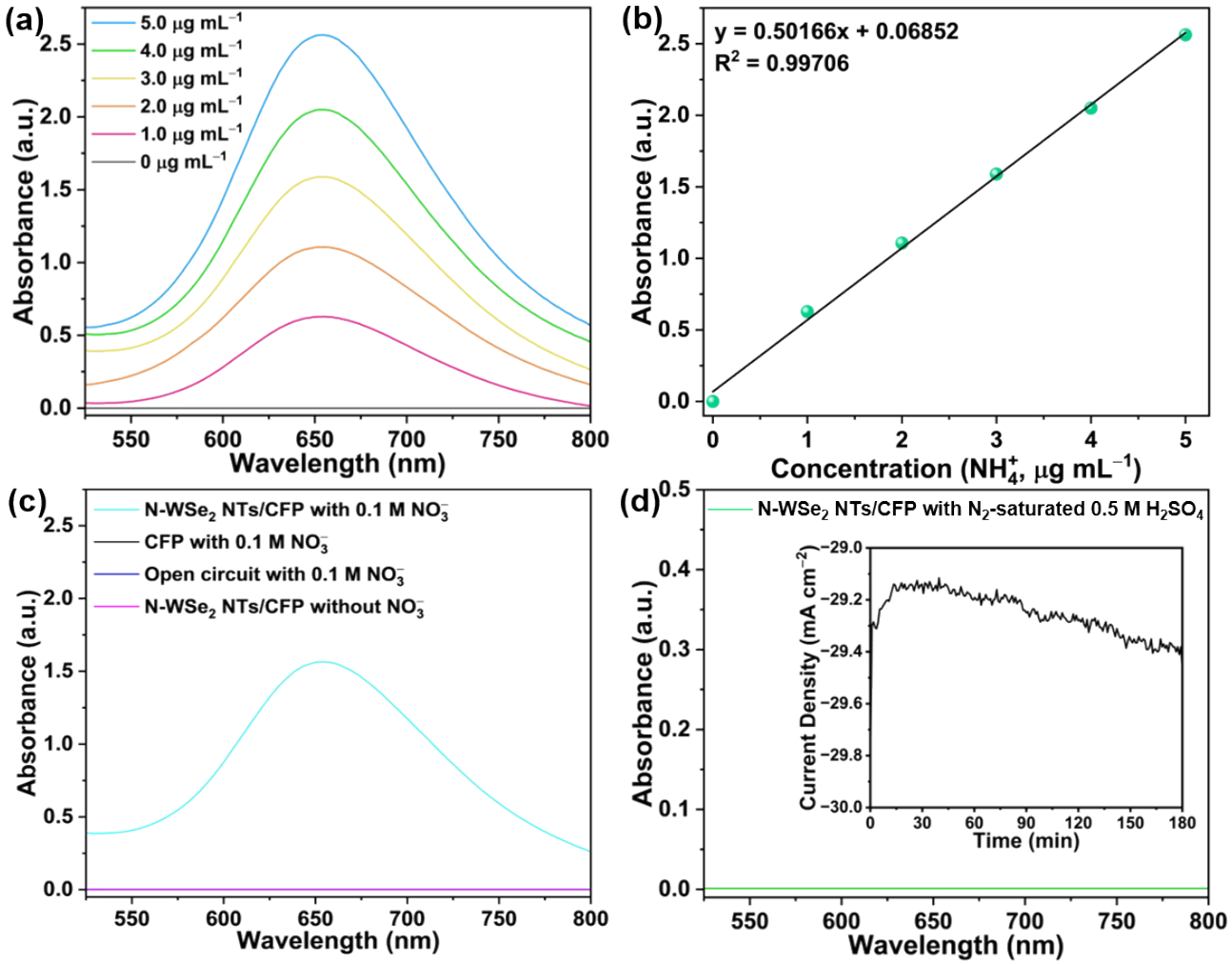

Figure S7. (a) The UV-vis absorption spectra of the aqueous solutions of NH_4^+ at a different concentration in 0.5 M H_2SO_4, (b) the corresponding calibration curve, (c) the electrolyte solutions obtained after electrolyzation for 30 s under different conditions, and (d) N-saturated 0.5 M H_2SO_4 after electrolyzation at −1.0 V_{RHE} for 180 min. The inset in panel (d) shows the corresponding chronoamperometry curve of electrolyzing N_2-saturated 0.5 M H_2SO_4 containing no NO_3^- at −1.0 V_{RHE} using N-WSe_2 NTs (5.1 at.% N)/CFP as the cathode.

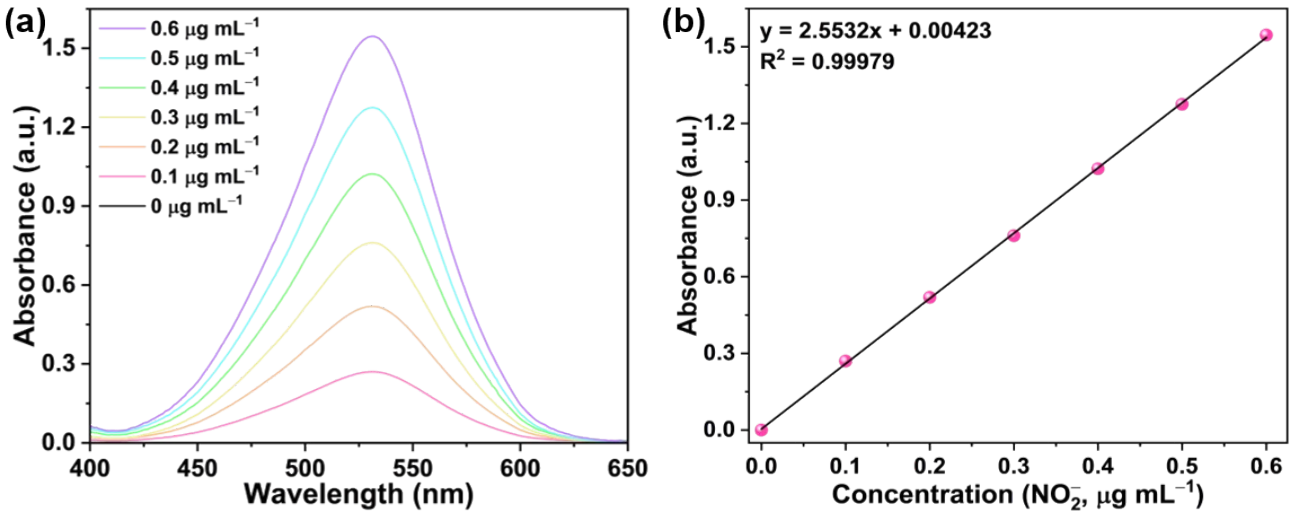

Figure S8. (a) The UV-vis absorption spectra of the aqueous solutions of nitrite (NO_2^-) at a different concentration in 0.5 M H_2SO_4 and (b) the corresponding calibration curve.

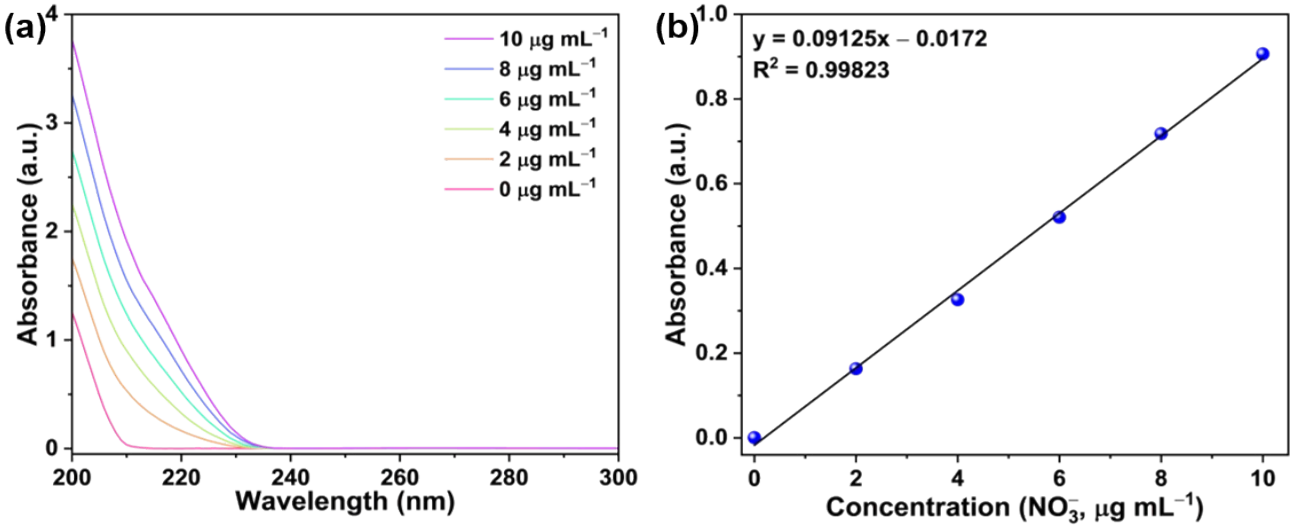

Figure S9. (a) The UV-vis absorption spectra of the aqueous solutions of nitrate (NO_3^-) at a different concentration in 0.5 M H_2SO_4, (b) the corresponding calibration curve.

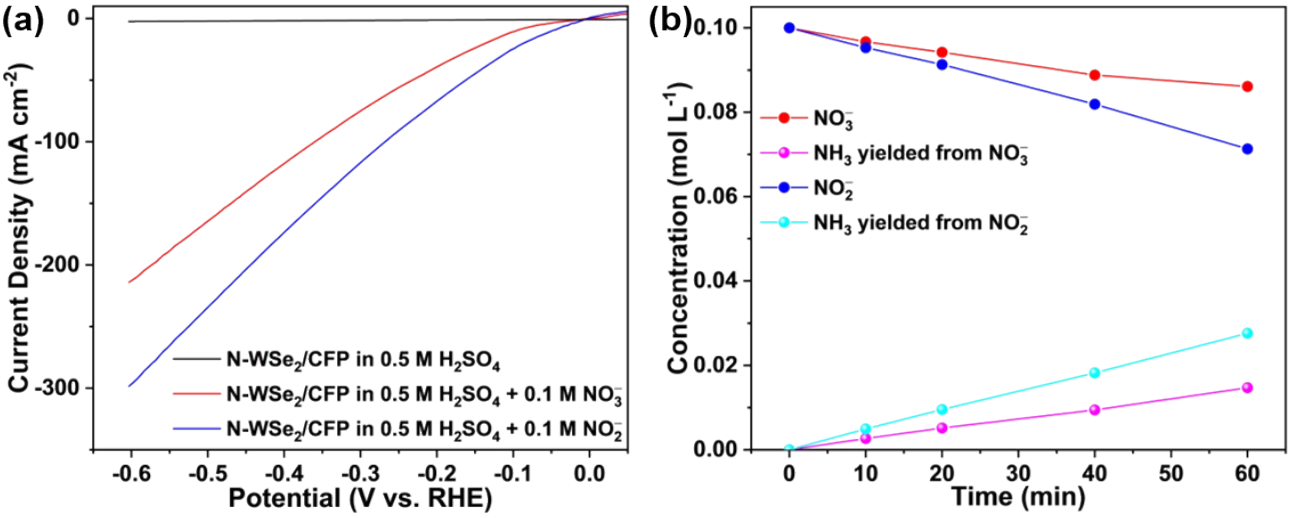

Figure S10. (a) Comparison of LSV curves recorded from the N-WSe_2/CPF cathode in a blank electrolyte (0.5 M H_2SO_4) and 0.5 M H_2SO_4 containing 0.1 M NO_3^-or 0.1 M NO_2^-. (b) Plots of concentration changes of NO_3^-, NO_2^-, and NH_3 as a function of time obtained using the N-WSe_2/CFP cathode at −0.5 V_{RHE}.

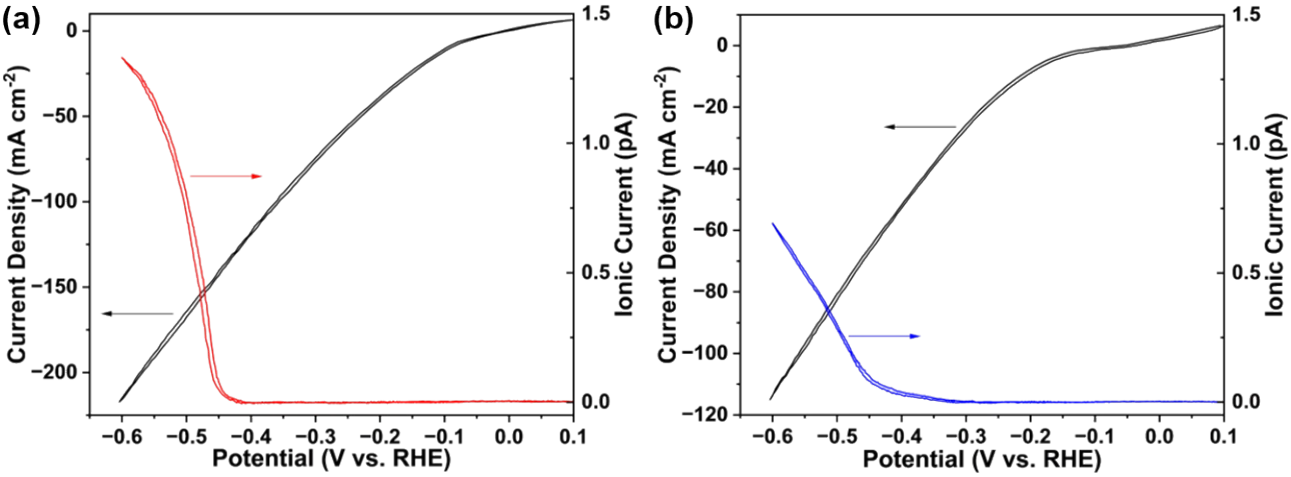

Figure S11. The NO_3^-RR faradaic current and ionic mass current for NO_2^- (m/z = 46) detection obtained during DEMS measurements of CV obtained (a) on the N-WSe_2 NTs surface and (b) WSe_2 NTs surface in 0.5 M H_2SO_4 containing 0.1 M $NaNO_3$.

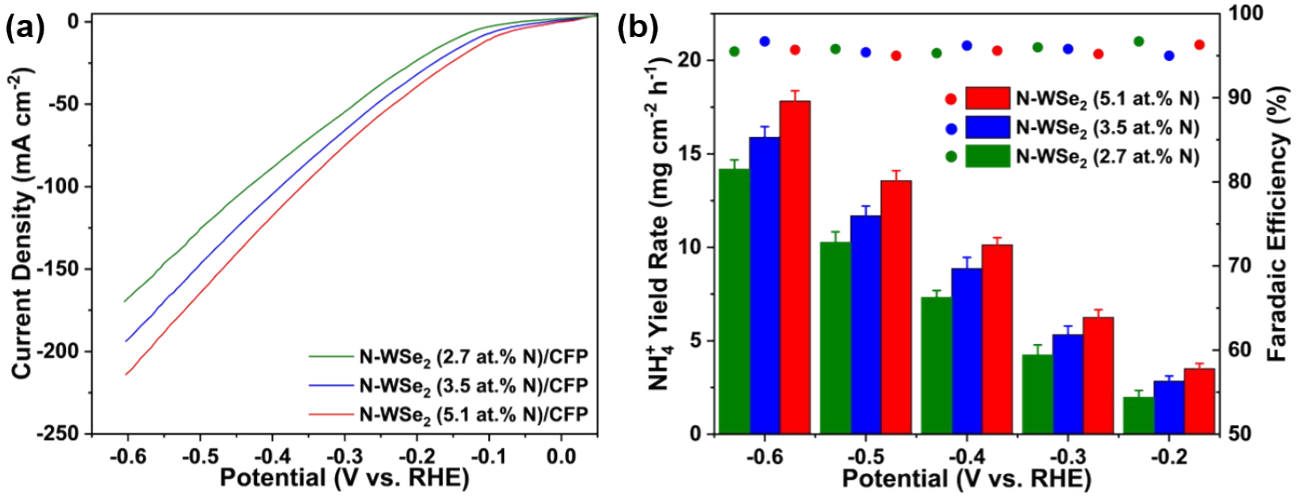

Figure S12. Comparison of (a) LSV curves and (b) NH_4^+ yield rates and FEs at different potentials of various N-WSe_2/CFP cathodes, including N-WSe_2 NTs (2.7 at./% N), N-WSe_2 NTs (3.5 at./% N), and N-WSe_2 NTs (5.1 at./% N), in 0.5 M H_2SO_4 containing 0.1 M NO_3^-.

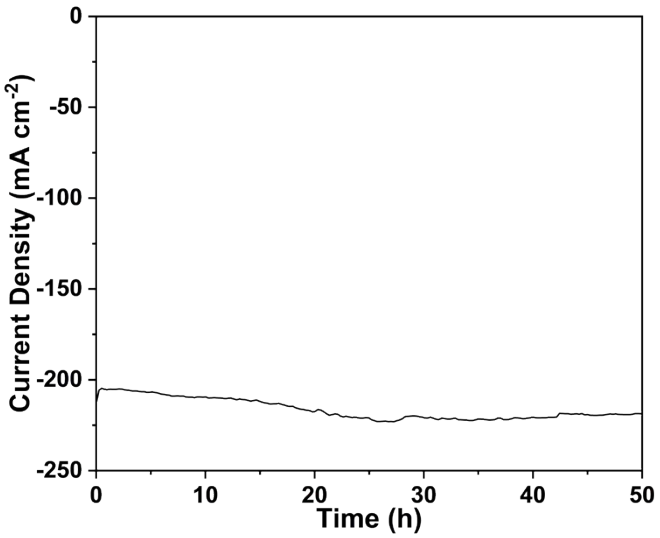

Figure S13. Chronoamperometry curve of the N-WSe_2 NTs (5.1 at.% N)/CFP at −0.6 V_{RHE} in 0.5 M H_2SO_4 containing 0.1 M NO_3^-.

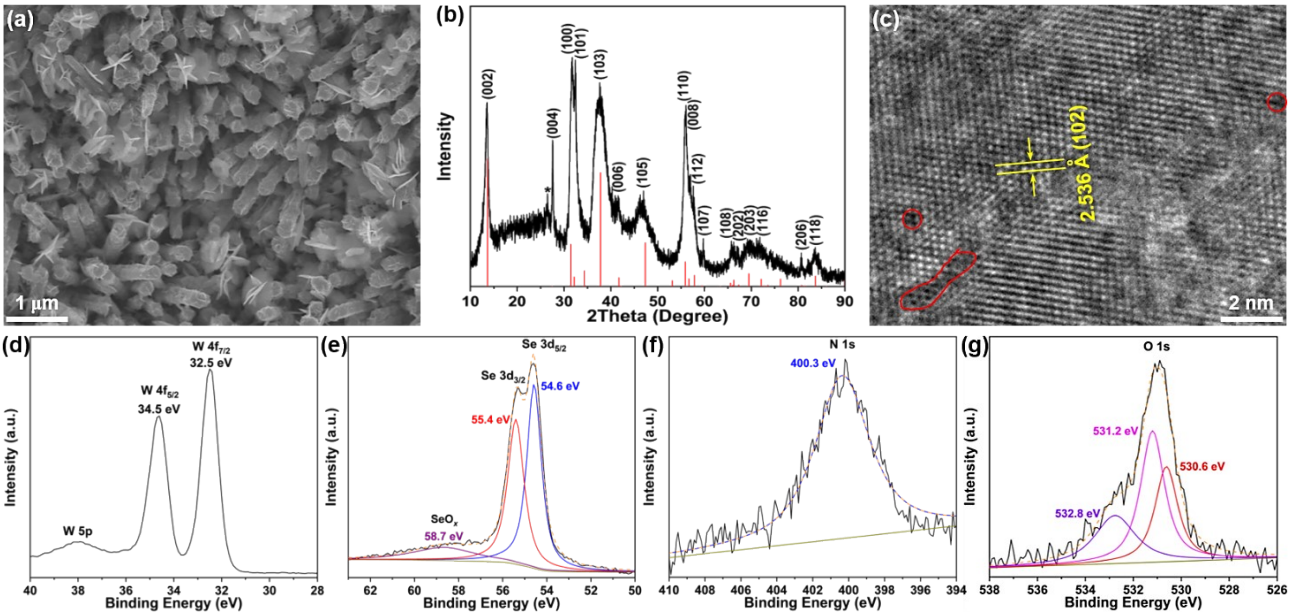

Figure S14. (a) SEM image, (b) XRD pattern, (c) HRTEM image, and (d–g) XPS (d) W 4f, (e) Se 3d, (f) N 1s, and (g) O 1s core-level spectra of the N-WSe_2 (5.1 at.% N) specimen after continuous 50 h electroreduction of NO_3^- in 0.5 M H_2SO_4 containing 0.1 M NO_3^-. The areas marked by circles and a loop in panel (c) denote the Se_v.

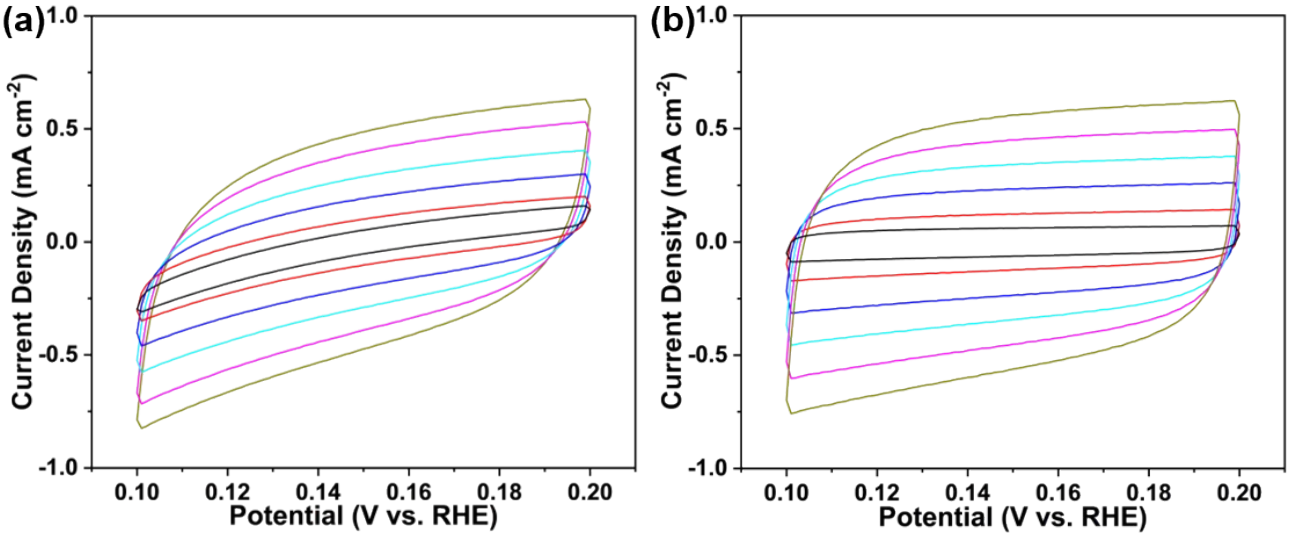

Figure S15. Cyclic voltammograms (CV) of (a) the WSe_2/CFP and (b) N-WSe_2/CFP in the non-Faradaic potential region of 0.1 to 0.2 V_{RHE} in 0.5 M H_2SO_4 electrolyte containing 0.1 M $NaNO_3$ at different scan rates, including 5, 10, 20, 30, 40, and 50 mV s^{-1}. The N-WSe_2 NTs present the approximately rectangular CV curves at various scan rates, implying their fast charge transfer capability and good conductivity.

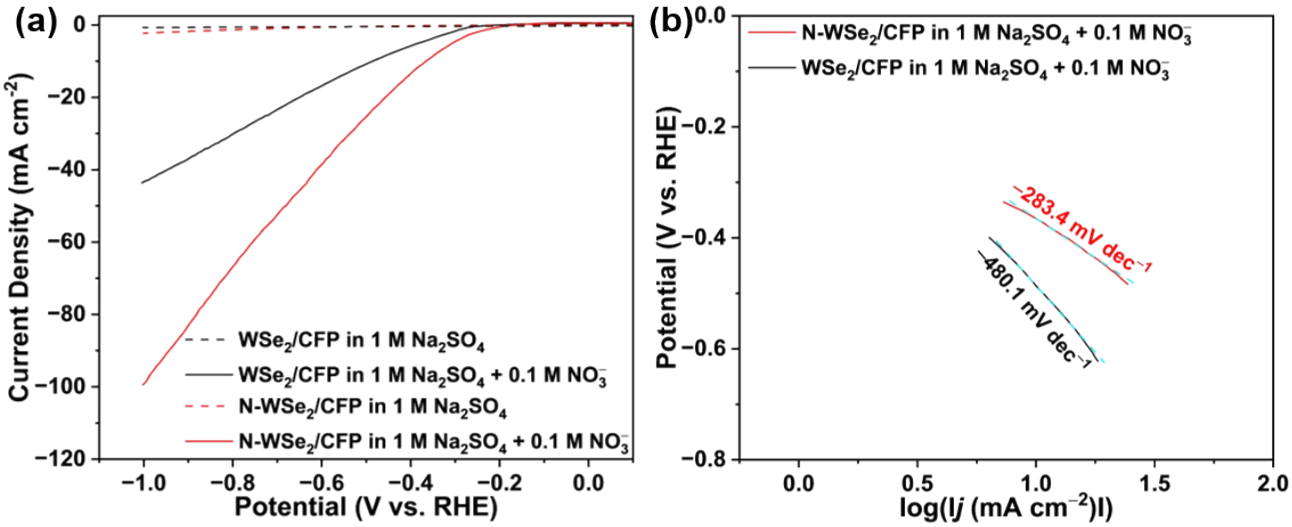

Figure S16. (a) LSV curves and (b) the corresponding Tafel plots of the WSe_2/CFP and N-WSe_2/CFP (5.1 at.% N) for the NO_3^-RR in 1 M Na_2SO_4 electrolyte containing 0.1 M $NaNO_3$ at a scan rate of 5 mV s^{-1} at ambient temperature.

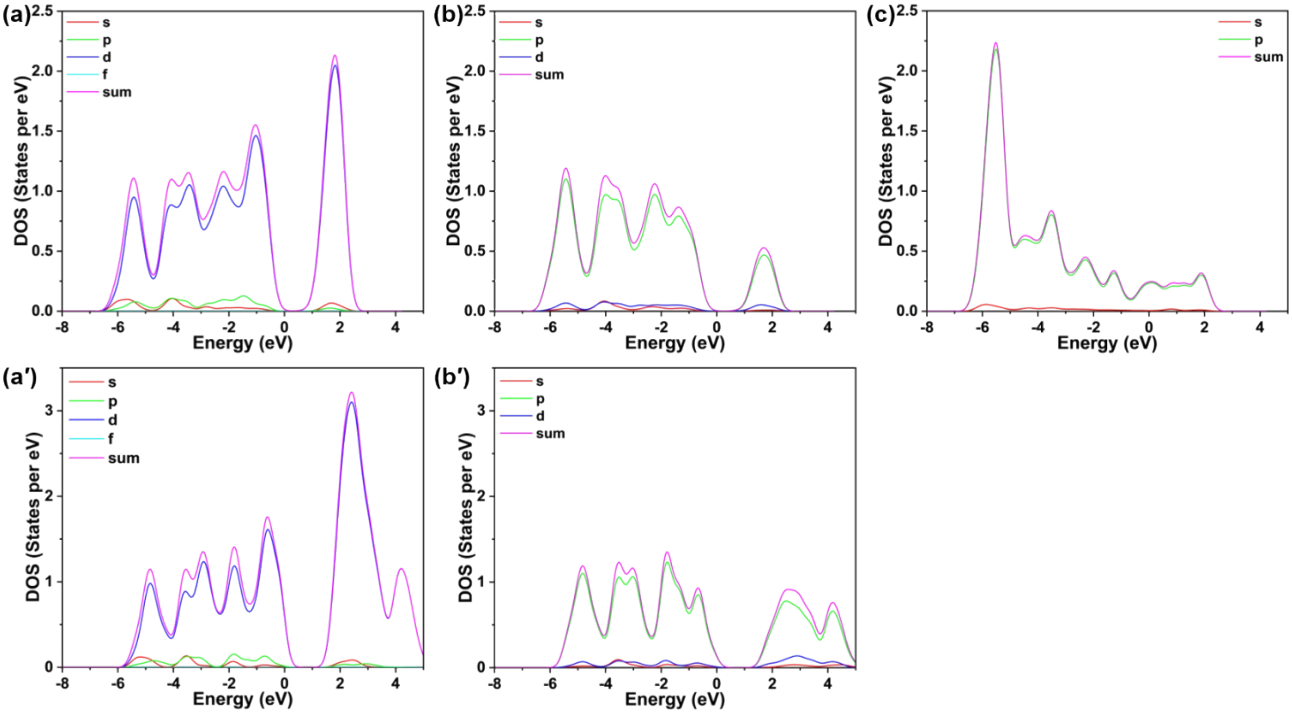

Figure S17. Partial density of states (PDOS) for (a and a′) W, (b and b′) Se, and (c) N in (a–c) N-WSe_2 and (a′ and b′) WSe_2.

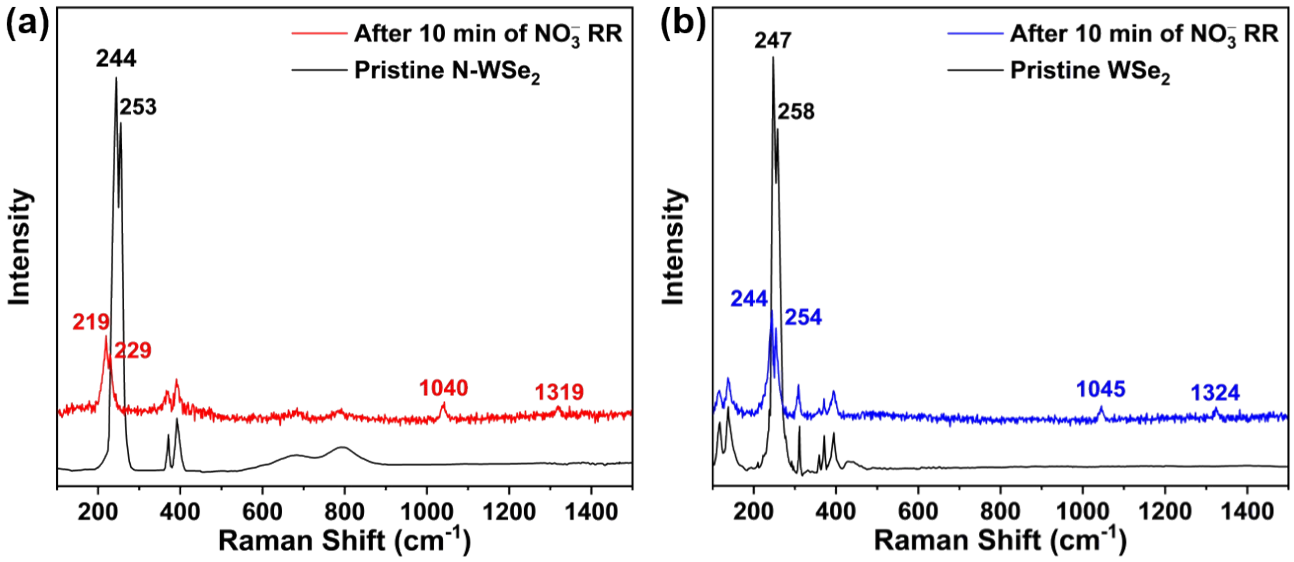

Figure S18. *In situ* Raman spectra of (a) the N-WSe_2 NTs (5.1 at.% N) and (b) WSe_2 NTs obtained at –0.5 V_{RHE} in 0.5 M H_2SO_4 electrolyte containing 0.1 M $NaNO_3$. For comparison, the corresponding initial counterpart is included in each panel.

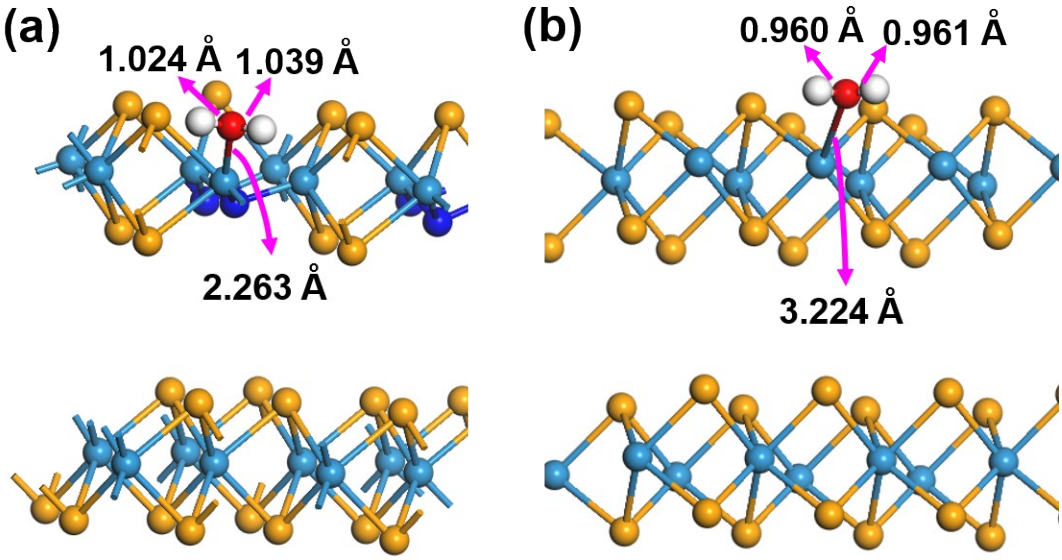

Figure S19. The optimized 3D geometric structure of the solvent water molecule adsorbed on the (a) N-WSe_2(001) and (b) WSe_2(001) surface. Red, blue, dark cyan, dark yellow, and white spheres represent O, N, W, Se, and H atoms, respectively. The solvent water can be slightly activated on N-WSe_2(001) by bonding to the W ion associated with a Se_v via the a′ level, as evidenced by the elongated O−H bonds ((1.024 and 1.039 Å) in comparison with free H_2O (0.96 Å). Compared to N-WSe_2(001), H_2O molecule can hardly be activated on WSe_2(001) since the distance (3.224 Å) between the W and O atoms is very far and the length (0.96 Å) of the O−H bonds for H_2O does not change with respect to free H_2O (0.96 Å).

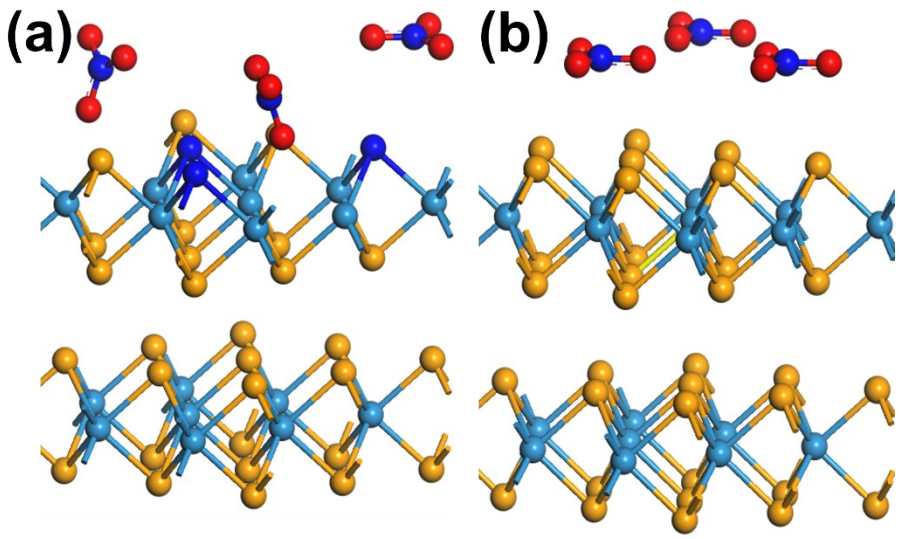

Figure S20. Adsorption configurations of NO_3^- on (a) N-WSe_2(001) and (b) WSe_2(001) surfaces obtained by Monte Carlo (MC) simulations. Red, blue, dark cyan, and dark yellow spheres represent O, N, W, and Se atoms, respectively. The specific adsorption energies of NO_3^- on (a) N-WSe_2(001) and (b) WSe_2(001) surfaces can be determined by the following equation:

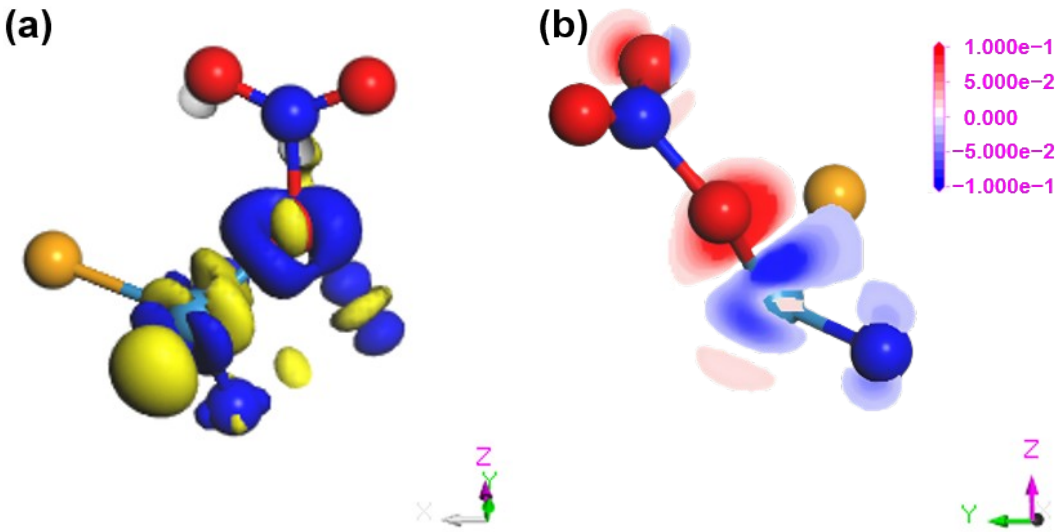

Figure S21. (a) Isosurface of electron density difference for N-WSe_2 viewed from [010] direction, in which the blue and yellow areas represent electron density gaining and depleting, respectively. (b) The corresponding electron localization function (ELF) contour plots on the (100) surface, where the red and blue regions denote the accumulation and depletion of charge density, respectively. Atoms: dark cyan, W; red, O; dark yellow, Se; blue, N.

Table S1. The chemical composition and excitonic peaks of the WSe_2 and various N-WSe_2 NTs

sample	EDX atomic percentage (at.%)				XPS atomic percentage (at.%)				excitonic peaks (nm)		
	W	Se	N	O	W	Se	N	O	A	B	C
WSe_2	33.1	66.4		0.5	33.2	66.5		0.3	765	590	450
N-WSe_2 (2.7 at.% N)	33.3	62.5	2.7	1.5	32.6	61.1	5.3	1.0	785	607	465
N-WSe_2 (3.5 at.% N)	33.8	61.3	3.5	1.4	31.9	60.7	5.2	2.2	790	617	475
N-WSe_2 (5.1 at.% N)	34.4	59.3	5.1	1.2	32.3	60.6	5.3	1.8	790	617	480

Table S2. Comparison of the performance of N-WSe_2 NTs with the recently reported electrocatalysts for NO_3^-RR under ambient conditions.[a]

electrocatalyst	electrolyte	potential (V_{RHE})	NH_3 yield rate (mg cm^{-2} h^{-1})	NH_3 FE (%)	ref
N-WSe_2 NTs	0.5 M H_2SO_4 + 0.1 M NO_3^-	−0.6	17.73	95.7	this work
Mo/H-CuW	0.5 M Na_2SO_4 + 0.05 M NO_3^-	−0.7	1.46	94.6	40
LC-rGO/BiNPs	0.01 M H_2SO_4 +0.5 M Na_2SO_4 + 0.01 M NO_3^-	−1.5	24.74	91.42	43
BCN@Cu/CNT	0.1 M KOH + 0.1 M NO_3^-	−0.6	3.44	95.32	68
Co_2B@Co_3O_4/TM	0.1 M PBS + 0.1 M NO_3^-	−1.0	8.57	97.0 (−0.7 V)	69
Co_3O_4-NS/Au-NWs	0.5 M K_2SO_4 + 0.05 M NO_3^-	−0.7	1.39	97.8 (−0.5 V)	70
1-Cu/CC	0.5 M Na_2SO_4 + 0.01 M NO_3^-	−0.9	1.66	75.6	71
$BiFeO_3$	0.1 M KOH + 0.1 M NO_3^-	−0.8	5.19	96.8 (−0.6 V)	72
Co_2AlO_4/CC	0.1 M PBS + 0.1 M NO_3^-	−0.7	7.90	92.6	73
FOSP-Cu	0.5 M Na_2SO_4 + 0.1 M NO_3^-	−0.266	1.73	93.91	74
Co_2–$Cu(OH)_2$	7 mM Na_2SO_4 + 50 ppm NO_3^-	−0.59	0.224	91.6	75
Co−30 %−CuO	1 M KOH + 0.1 M NO_3^-	−0.4	9.25	93.9	76

[a] Although the LC-rGO/BiNPs shows a higher NH_4^+ yield rate at −1.5 V_{RHE} (entry 2), the corresponding large reduction potential is associated with a high energy input and the occurrence of severe competing HER. In addition, cupric hydroxide and oxide can not be stable at the potentials shown in Table S2 according to the pH-potential diagrams of Cu-O-H_2O system, although they show a high activity to some degree.

Table S3. The reaction energy (ΔE), zero point energy corrections (E_{ZPE}), and entropic contributions ($T\Delta S$) of closed shell molecules during the NO_3^-RR process on the N-WSe_2(001) and WSe_2(001) surfaces at T = 298.15 K.

intermediate species	catalyst surfaces	ΔE (eV)	E_{ZPE}	$T\Delta S$
*NO_3	N-WSe_2(001)	−2.54	0.36	0.25
	WSe_2(001)	−1.45	0.35	0.25
*NO_2	N-WSe_2(001)	−2.13	0.27	0.25
	WSe_2(001)	−0.90	0.28	0.25
*NO	N-WSe_2(001)	−4.32	0.12	0.21
	WSe_2(001)	−3.17	0.11	0.22
*N	N-WSe_2(001)	−5.15	0.07	0.16
	WSe_2(001)	−4.26	0.07	0.18
*NH	N-WSe_2(001)	−5.88	0.32	0.31
	WSe_2(001)	−4.55	0.32	0.30
*NH_2	N-WSe_2(001)	−6.65	0.64	0.36
	WSe_2(001)	−5.19	0.63	0.36
*NH_3	N-WSe_2(001)	−7.57	0.98	0.43
	WSe_2(001)	−5.93	0.98	0.41

References

1. N. M. Tzollas, G. A. Zachariadis, A. N. Anthemidis and J. A. Stratis, A new approach to indophenol blue method for determination of ammonium in geothermal waters with high mineral content. *Intern. J. Environ. Anal. Chem*., 2010, **90**, 115–126.